JOURNAL OF GEOPHYSICAL RESEARCH, VOL. 106, NO. B8, PAGES 16,339-16,355, AUGUST 10, 2001

Inversion for parameters of tensile earthquakes

Václav Vavryčuk[1]

Centro de Pesquisa em Geofísica e Geologia, Instituto de Física, Universidade Federal da Bahia
Salvador, Brazil

Abstract. The tensile source model generalizes the shear source model by assuming that the slip vector can be arbitrarily oriented with respect to the fault and is not constrained to lie within the fault plane. The proposed inversion for the parameters of tensile sources is based on the evaluation of the isotropic (ISO), compensated linear vector dipole (CLVD), and double-couple (DC) components in seismic moment tensors. The most significant parameters inverted are the λ/μ ratio at the fault (denoted as the κ parameter) and the inclination α of the slip vector from the fault. The κ parameter is significant for discriminating noisy moment tensors of shear earthquakes from those of tensile earthquakes. The inclination α can be accurately determined from the DC component in the moment tensor because the DC component rapidly decreases with increasing α. For example, the inclination of 20° causes DC being ~50-60% only. The inversion is applied to earthquakes which occurred in January 1997 in West Bohemia, Czech Republic. It is shown that some of these earthquakes display tensile faulting. The κ parameter is ~0.1. The inclination of the slip from the fault attains values of up to 20°. This inclination is a result of tensile traction and reduced shear traction along the fault and high-fluid pressure in the region.

1. Introduction

Most earthquakes are caused by shear faulting and display a double-couple (DC) mechanism. Non-double-couple (non-DC) mechanisms are much rarer and are of various origins. They can be spurious artefacts of inaccurate moment tensor inversion [*Kuge and Lay*, 1994] or of inadequacy of the source or medium models used in the inversion [*Sipkin*, 1986; *Šílený and Vavryčuk*, 2000]. They can also be real, reflecting specific earthquake source processes (for reviews, see *Frohlich* [1994], *Julian et al.* [1998], and *Miller et al.* [1998]). The non-DC mechanisms have been reported for volcanic earthquakes caused by magma intrusions, for mining tremors connected to volume changes, for deep-focus earthquakes, or in relation to landslides.

One large family of non-DC earthquakes are earthquakes with tensile faulting or with combined tensile and shear faulting. Hereinafter they are referred to as "tensile earthquakes." A tensile earthquake is described by a slip vector pointing in an arbitrary direction not necessarily restricted to lie within the fault plane (see Figure 1). Hence the slip vector deviates from the fault and causes its opening or closing. Opening of faults is important also in crack dynamics because a small tensile component in the rupture process can probably explain the weakness of major active faults and the heat flow paradox [*Brune et al.*, 1993; *Anooshehpoor and Brune*, 1994]. Tensile earthquakes have been studied theoretically [*Walter and Brune*, 1993] as well as in laboratory experiments simulating the intersection of shear and tensile faults [*Brace et al.*, 1966, *Špičák*, 1988; *Scholz*, 1990]. Tensile earthquakes in situ have been reported to occur particularly in geothermal and volcanic areas [*Shimizu et al.*, 1987; *Foulger*, 1988a, 1988b; *Ross et al.*, 1996; *Julian et al.*, 1997], which are rich in fluids. Fluids are important for the generation of tensile earthquakes since they can cancel out the compressive lithostatic stress at depth in the Earth, which tends to prevent tensile faulting [*Julian et al.*, 1998].

In this paper, tensile earthquakes are studied by means of moment tensors. Moment tensors mathematically describe any source mechanisms and are conventionally decomposed into three components [*Knopoff and Randall*, 1970]: isotropic (ISO), compensated linear vector dipole (CLVD), and double-couple (DC). The ISO, CLVD, and DC components represent equivalent forces for various types of the source. The pure DC component is associated with shear faulting, the pure ISO component is associated with explosive or implosive sources, and both ISO and CLVD components are produced by the opening or closing of faults. Hence the values of the CLVD and ISO estimate the deviation of the equivalent forces from the DC mechanism. Although the decomposition into ISO, CLVD, and DC quantifies the non-DC mechanisms in a well-defined and unambiguous way, this procedure is a rather mathematical one and yields poor information on the physical processes in the source. For example, if we detect a mixture of the ISO, CLVD, and DC components in a moment tensor, the physical interpretation of the source is difficult. Therefore this decomposition is adopted as the starting point for further evaluation of the parameters that are more directly connected to the model of tensile earthquakes.

The inversion problem for parameters of tensile earthquakes is studied theoretically, as well as numerically. In

[1] On leave from Geophysical Institute, Academy of Sciences of the Czech Republic, Prague, Czech Republic.

Paper number 2001JB000372.
0148-0227/01/2001JB000372$09.00

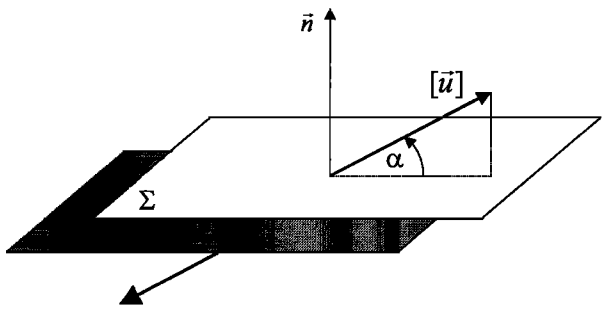

Figure 1. A model for the tensile earthquake. Σ is the fault plane, **n** is the normal to the fault, [**u**] is the slip vector at the fault, and α is the inclination of the slip vector from the fault.

theory, I show procedures how to invert for the parameters using the ISO, CLVD, and DC components. In numerical modeling, a problem of distinguishing between the spurious and real non-DC mechanisms is discussed because we have to be careful not to misinterpret the errors in the moment tensors of shear earthquakes in favor of the model of tensile earthquakes. Finally, the inversion proposed is applied to earthquakes that occurred during the January 1997 earthquake swarm in West Bohemia, Czech Republic [*Horálek et al.*, 2000b], which is a geothermally active region characteristic by the occurrence of earthquake swarms. Some of the earthquakes are shown to be highly non-DC and consistent with the model of tensile faulting. The analysis of tectonic stress in the region indicates that the tensile earthquakes occur along the faults characterized by tensile traction together with significantly reduced shear traction.

2. Theory

2.1. Moment Tensor for a Tensile Source

Seismic moment tensor **M** for a point source at a fault with isotropic behaviour is expressed as [*Aki and Richards*, 1980, equation 3.20]

$$M_{kl} = \lambda [u_i] n_i \delta_{kl} + \mu \left([u_k] n_l + [u_l] n_k \right), \tag{1}$$

where λ and μ are Lamé coefficients at the fault, δ_{kl} is the Kronecker delta, [**u**] is the slip vector, and **n** is the normal of the fault. If we assume

$$\mathbf{n} = (0,0,1)^T, \quad [\mathbf{u}] = u(\cos\alpha, 0, \sin\alpha)^T,$$

the moment tensor takes the following form:

$$\mathbf{M} = u \begin{bmatrix} \lambda \sin\alpha & 0 & \mu\cos\alpha \\ 0 & \lambda\sin\alpha & 0 \\ \mu\cos\alpha & 0 & (\lambda + 2\mu)\sin\alpha \end{bmatrix}, \tag{2}$$

where $\alpha \in \langle -90°, 90° \rangle$ denotes the inclination of slip [**u**] from the fault. For $\alpha > 0°$ the source is tensile, and for $\alpha < 0°$ the source is compressive. The pure shear source is defined by $\alpha = 0°$, while the pure tensile and compressive sources are defined by values $\alpha = \pm 90°$, respectively. Moment tensor **M** can be diagonalized in the principal axis system as follows [*Dufumier and Rivera*, 1997]:

$$\mathbf{M} = u \begin{bmatrix} \lambda\sin\alpha - \mu(1-\sin\alpha) & 0 & 0 \\ 0 & \lambda\sin\alpha & 0 \\ 0 & 0 & \lambda\sin\alpha + \mu(1+\sin\alpha) \end{bmatrix}. \tag{3}$$

The trace of **M** reads

$$\mathrm{tr}(\mathbf{M}) = (3\lambda + 2\mu) u \sin\alpha. \tag{4}$$

It follows from the stability conditions [*Backus*, 1962]

$$\mu > 0, \quad \frac{\lambda}{\mu} > -\frac{2}{3}, \tag{5}$$

that term $3\lambda + 2\mu$ in (4) is always positive and the sign of the trace of **M** depends on angle α only. Hence the trace of **M** is positive for tensile sources and negative for compressive sources.

2.2. Decomposition of the Moment Tensor

Moment tensor **M** is decomposed into the isotropic (ISO), compensated linear vector dipole (CLVD), and double-couple (DC) components. The decomposition reads [*Knopoff and Randall*, 1970; *Jost and Hermann*, 1989]

$$\mathbf{M} = \mathbf{M}^{\mathrm{ISO}} + \mathbf{M}^{\mathrm{CLVD}} + \mathbf{M}^{\mathrm{DC}}, \tag{6}$$

where

$$\mathbf{M}^{\mathrm{ISO}} = \frac{1}{3}\mathrm{tr}(\mathbf{M}) \begin{bmatrix} 1 & 0 & 0 \\ 0 & 1 & 0 \\ 0 & 0 & 1 \end{bmatrix},$$

$$\mathbf{M}^{\mathrm{CLVD}} = |\varepsilon| \, M^*_{|\max|} \begin{bmatrix} -1 & 0 & 0 \\ 0 & -1 & 0 \\ 0 & 0 & 2 \end{bmatrix},$$

$$\mathbf{M}^{\mathrm{DC}} = (1 - 2|\varepsilon|) M^*_{|\max|} \begin{bmatrix} -1 & 0 & 0 \\ 0 & 0 & 0 \\ 0 & 0 & 1 \end{bmatrix}.$$

The sum of the ISO and CLVD components is called the non-DC component of **M**. The sum of the CLVD and DC components is called the deviatoric moment $\mathbf{M}^*$. Parameter ε measures the size of CLVD relative to DC [*Sipkin*, 1986; *Kuge and Lay*, 1994; *Julian et al.*, 1998, equation (18)] and is defined as

$$\varepsilon = -\frac{M^*_{|\min|}}{\left| M^*_{|\max|} \right|}, \tag{7}$$

where $M^*_{|\max|}$ and $M^*_{|\min|}$ are the eigenvalues of deviatoric moment $\mathbf{M}^*$ with the maximum and minimum absolute values, respectively. For a pure DC, $\varepsilon = 0$, and for a pure CLVD, $\varepsilon = \pm 0.5$. Parameter ε is positive for tensile sources and negative for compressive sources.

2.3. Percentage of the ISO, CLVD, and DC Components

The calculation of the DC relative to the CLVD percentage is a standard procedure [*Sipkin*, 1986; *Kuge and Lay*, 1994; *Julian et al.*, 1998] that utilizes the value of parameter ε defined in (7). The calculation of the ISO percentage, however, is less common and not unified; hence several

alternative formulas are used [see *Šílený and Pšenčík*, 1995; *Dahm*, 1996]. In this paper, the following formulas for the ISO, CLVD, and DC percentages are suggested and applied:

$$c^{\mathrm{ISO}} = \frac{1}{3}\frac{\mathrm{tr}(\mathbf{M})}{\left|M_{|\max|}\right|}\,100\%, \tag{8a}$$

$$c^{\mathrm{CLVD}} = 2\varepsilon\left(100\% - \left|c^{\mathrm{ISO}}\right|\right), \tag{8b}$$

$$c^{\mathrm{DC}} = 100\% - \left|c^{\mathrm{ISO}}\right| - \left|c^{\mathrm{CLVD}}\right|, \tag{8c}$$

where $M_{|\max|}$ denotes that eigenvalue of **M**, which has the maximum absolute value and ε is defined by (7). The DC percentage is always positive, and the ISO and CLVD percentages are positive for tensile sources, but negative for compressive sources. The sum of the absolute values of the DC and non-DC percentages is 100%.

Inserting (3) and (4) into (8), we obtain

$$c^{\mathrm{ISO}} = \mathrm{sign}(\alpha)\frac{\left(\kappa+\frac{2}{3}\right)\sin|\alpha|}{(\kappa+1)\sin|\alpha|+1}\,100\%, \tag{9a}$$

$$c^{\mathrm{CLVD}} = \mathrm{sign}(\alpha)\frac{4}{3}\frac{\sin|\alpha|}{(\kappa+1)\sin|\alpha|+1}\,100\%, \tag{9b}$$

$$c^{\mathrm{DC}} = \frac{(1-\sin|\alpha|)}{(\kappa+1)\sin|\alpha|+1}\,100\%, \tag{9c}$$

where κ represents the λ/μ ratio. This ratio describes the behavior of the fault but not of the medium surrounding the fault. Since the fault is an interface (or thin zone) of weakness in the medium, we can expect the rheological properties of the fault to be distinctly different from those of the surrounding medium. Therefore the λ/μ ratio at the fault cannot be identified with the standard λ/μ ratio, which is calculated, for example, from the propagation velocities of seismic waves. Neither can it be estimated by adopting some standard values, for example, using the classical relation $\lambda = \mu$, which is equivalent to $v_P/v_S = \sqrt{3}$. Some authors ignore this fact [see *Dufumier and Rivera*, 1997], but this omission can lead to misinterpretations of the source parameters. Therefore, in order to avoid confusion and to distinguish clearly between the two different ratios mentioned, the λ/μ ratio at the fault is denoted as parameter κ. Obviously, the retrieval of κ can provide information on the physical conditions at the fault.

Figure 2 shows the ISO, CLVD, and DC percentages as a function of α. All three functions are monotonic in the interval of angles $\alpha \in \langle 0°, 90°\rangle$: the DC percentage decreases, while the ISO and CLVD percentages increase. The form of the DC curve is little affected by the κ parameter. This parameter mainly affects the relative amount of the ISO versus CLVD components in **M**. For example, the percentage of the ISO component is higher than that of CLVD for $\kappa = 1$, but the reverse is true for $\kappa = 0.2$ (see Figure 2). Comparing (9a) and (9b), we can readily put

$$\frac{c^{\mathrm{ISO}}}{c^{\mathrm{CLVD}}} = \frac{3}{4}\kappa + \frac{1}{2}. \tag{10}$$

Hence the $c^{\mathrm{ISO}}/c^{\mathrm{CLVD}}$ ratio is independent of inclination α of the slip from the fault. This is a basic advantage of decomposition (8). For example, if we calculate the percentage of the ISO component as (see Figure 3)

$$c^{\mathrm{ISO}} = \frac{1}{3}\frac{[\mathrm{tr}(\mathbf{M})]^2}{\mathrm{tr}(\mathbf{M}^2)}\,100\%, \tag{11}$$

and the percentage of the CLVD and DC using (8b) and (8c), the independence of the $c^{\mathrm{ISO}}/c^{\mathrm{CLVD}}$ ratio on angle α is lost (see Figure 4). This property, however, is important, because it can be exploited in estimating the κ parameter from a set of earthquakes, which display different values of inclination α.

Equation (10) holds for positive as well as negative values of α. It follows from stability conditions (5) that the $c^{\mathrm{ISO}}/c^{\mathrm{CLVD}}$ ratio must always be positive. In other words, the ISO and CLVD percentages must always be of the same sign.

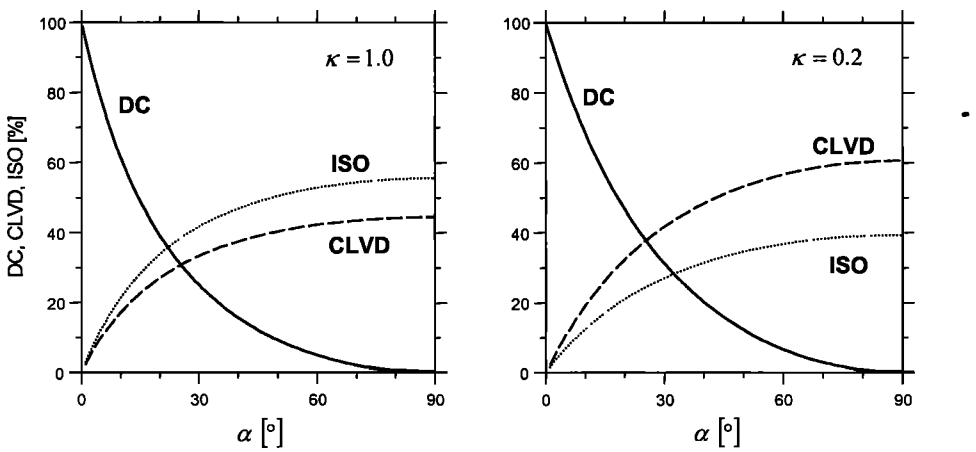

Figure 2. The percentage of the ISO, CLVD, and DC components calculated from equations (8a)-(8c) as a function of the inclination α of the slip vector from the fault. The functions are shown (left) for $\kappa = 1$ and (right) for $\kappa = 0.2$.

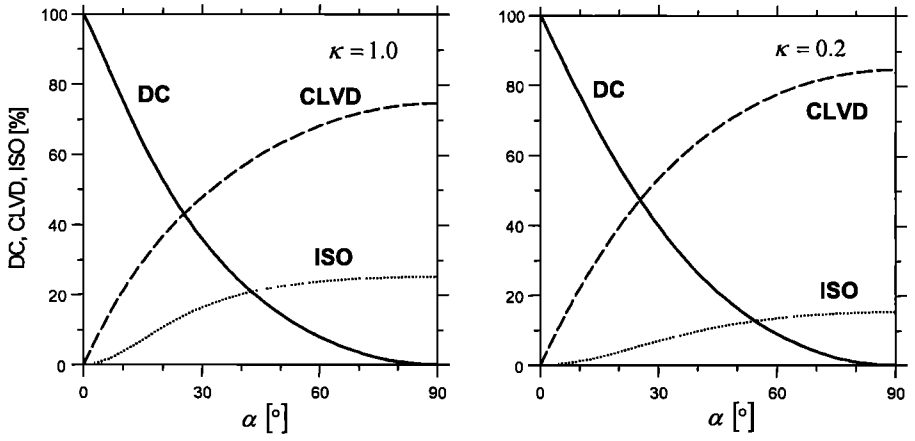

Figure 3. The percentage of the ISO, CLVD, and DC components calculated from equations (8b) and (8c) and (11) as a function of the inclination α of the slip vector from the fault. The functions are shown (left) for $\kappa = 1$ and (right) for $\kappa = 0.2$.

2.4. Determination of the Source Parameters

Once moment tensor **M** in (1) is retrieved from the actual data, it can be inverted to obtain the following parameters: normal of the fault **n**, slip direction **N**, and products λu and μu. Obviously, parameters λ and μ cannot be separated from slip u. Instead of determining the above parameters, it is more practical, however, to invert for the following alternative set of parameters: orientations of P and T axes, parameter κ, and inclination α of the slip from the fault. The κ parameter and inclination α are the most important parameters because they play a crucial role in discriminating shear and tensile earthquakes. To determine these two parameters, we can proceed in the following ways.

2.4.1. Direct evaluation from eigenvalues of moment tensor M. We can directly calculate the κ parameter and inclination α from moment tensor **M** and its deviatoric part $\mathbf{M}^*$ as follows [*Dufumier and Rivera*, 1997]:

$$\kappa = \frac{2}{3}\left(\frac{\mathrm{tr}(\mathbf{M})/3}{M^*_{\max} + M^*_{\min}} - 1\right), \tag{12}$$

$$\alpha = \arcsin\left(3\frac{M^*_{\max} + M^*_{\min}}{\left|M^*_{\max}\right| + \left|M^*_{\min}\right|}\right), \tag{13}$$

where $M^*_{\max}$ and $M^*_{\min}$ are defined as the maximum and minimum deviatoric eigenvalues (do not confuse with the deviatoric eigenvalues with maximum and minimum absolute values $M^*_{|\max|}$ and $M^*_{|\min|}$). Note that (12) is presented by *Dufumier and Rivera* [1997] with an error: in their formula the term tr(**M**) is not divided by factor 3. Since the denominator $M^*_{\max} + M^*_{\min}$ vanishes for $\alpha = 0$, formula (12) becomes numerically unstable for small inclinations α. This means that κ cannot be retrieved safely from **M** for

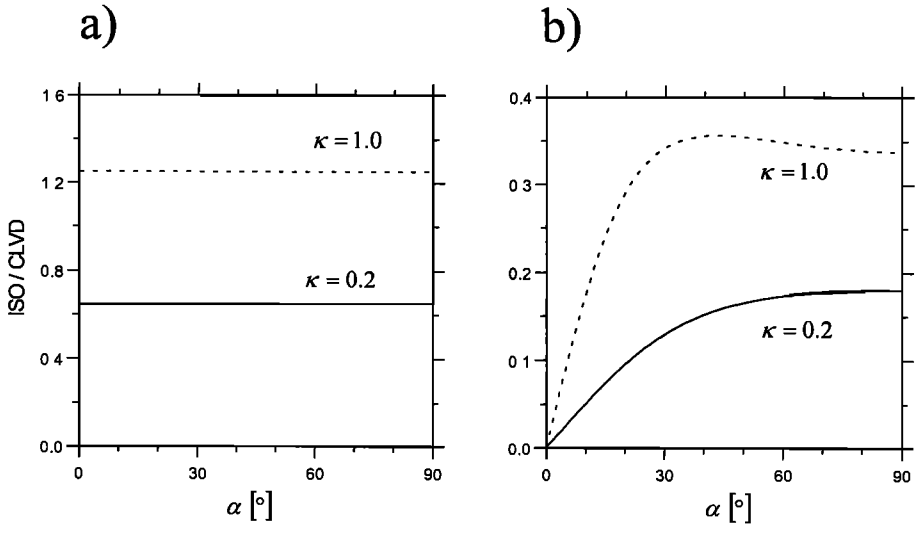

Figure 4. A comparison of the ISO/CLVD ratios as a function of α for two different ISO-CLVD-DC decompositions. (a) The ISO component was calculated using equation (8a). (b) The ISO component was calculated using equation (11). The functions are shown for $\kappa = 1$ and for $\kappa = 0.2$.

sources, which are very close to shear dislocation. This is obvious because **M** contains no information on λ for pure shear source.

2.4.2. Calculation from the percentage of ISO, CLVD, and DC components. We can calculate the κ parameter and inclination α from the relative amounts of ISO, CLVD and DC components of **M**.

First, we can check the compatibility of **M** with the model of earthquake source (1) by calculating the $c^{\mathrm{ISO}}/c^{\mathrm{CLVD}}$ ratio. As mentioned above, the ratio must always be positive. A negative $c^{\mathrm{ISO}}/c^{\mathrm{CLVD}}$ ratio could indicate either the presence of numerical errors in **M**, which can be generated during inversion from the actual noisy data or that the model used is not adequate to describe the particular seismic source.

Second, we can estimate the κ parameter from (10):

$$\kappa = \frac{4}{3}\left(\frac{c^{\mathrm{ISO}}}{c^{\mathrm{CLVD}}} - \frac{1}{2}\right). \tag{14}$$

We can see that κ is a linear function of the $c^{\mathrm{ISO}}/c^{\mathrm{CLVD}}$ ratio. If the tensile source produces no ISO component, then κ equals $-2/3$, which is the lowest physically acceptable limit for this parameter. The positive $c^{\mathrm{ISO}}/c^{\mathrm{CLVD}}$ ratio yields condition $\kappa > -2/3$, and the negative $c^{\mathrm{ISO}}/c^{\mathrm{CLVD}}$ ratio is equivalent to unphysical values of κ, $\kappa < -2/3$.

Third, inclination α can be estimated from the percentage of the ISO, CLVD, or DC components. Once the κ parameter is fixed, the percentage of the ISO, CLVD, and DC components is a unique function of inclination α (see Figure 2). Using (9a)-(9c), we can readily put

$$\alpha^{\mathrm{ISO}} = \mathrm{sign}\left(c^{\mathrm{ISO}}\right)\mathrm{asin}\frac{\left|c^{\mathrm{ISO}}\right|}{\left(\kappa+\frac{2}{3}\right)\left(100\%-\left|c^{\mathrm{ISO}}\right|\right)-\frac{1}{3}\left|c^{\mathrm{ISO}}\right|}, \tag{15a}$$

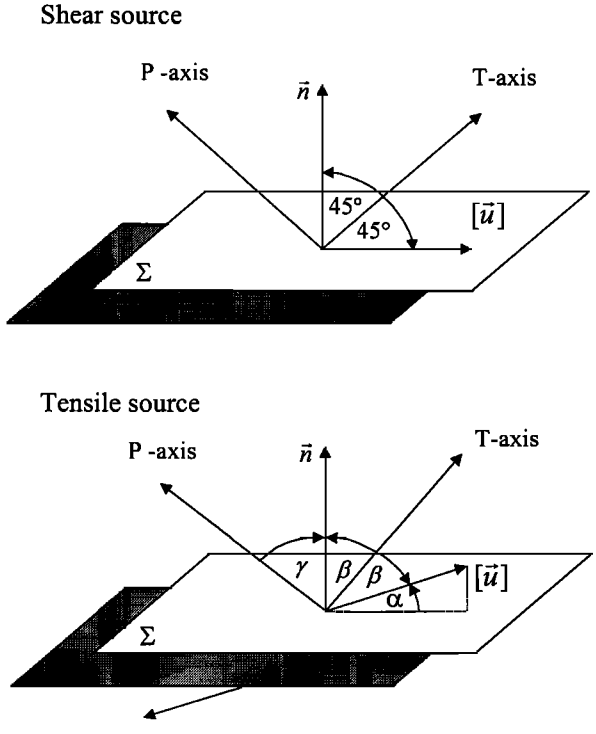

Figure 5. P and T axes for the (top) shear and (bottom) tensile sources.

$$\alpha^{\mathrm{CLVD}} = \mathrm{sign}\left(c^{\mathrm{CLVD}}\right)\mathrm{asin}\frac{\left|c^{\mathrm{CLVD}}\right|}{\frac{4}{3}100\%-\left|c^{\mathrm{CLVD}}\right|(\kappa+1)}, \tag{15b}$$

$$\alpha^{\mathrm{DC}} = \mathrm{sign}\left(c^{\mathrm{CLVD}}\right)\mathrm{asin}\frac{100\%-c^{\mathrm{DC}}}{100\%+c^{\mathrm{DC}}(\kappa+1)}. \tag{15c}$$

The sign of α^{DC} in (15c) is controlled by the sign of c^{CLVD}, but in principle, the sign of c^{ISO} can also be used. Since we cannot determine uniquely the sign of α^{DC} from the percentage of DC, we have to use additional information by incorporating either the sign of c^{ISO} or c^{CLVD}.

All three formulas for inclination α (15a)-(15c) are equivalent if data are noise free. They are even equivalent to (13), where α is calculated directly from the eigenvalues of **M**. Similarly, (12) and (14) yield identical results when no noise is present in **M**. However, the mentioned equations behave in a different way if moment **M** is noisy. In section 3, the different behavior of these formulas will be studied by numerical modeling.

Figure 2 indicates that the percentages of ISO, CLVD, and DC components are very sensitive to α, if α is small. This implies that even a source, which is very close to shear dislocation, can produce rather low DC and high non-DC components. Therefore, if moment **M** is well retrieved and the values of the ISO, CLVD, and DC percentages are reliable, very small inclinations α of the slip from the fault can be accurately detected. Figure 2 also indicates that even a remarkable reduction of the DC percentage to ~50-60% can be successfully explained by tensile faulting, the slip inclination being only of 20°.

2.5. Correction for a True Fault Orientation and Slip Direction

Moment tensor **M** diagonalizes in the coordinate system connected to the pressure (P) and tension (T) axes, which are mutually perpendicular. These axes bisect the angle between the fault normal and the slip vector. For a shear source the fault normal and the slip vector are mutually perpendicular; hence the P and T axes are inclined from the fault plane by an angle of 45° (see Figure 5, top). However, for a tensile source the fault normal and the slip vector deviate mutually by angle $90°-\alpha$ (see Figure 5, bottom), and the angles between the fault normal and the P and T axes are no longer 45°. The angle between the T axis and the fault normal is $\beta = 45° - \alpha/2$, and the angle between the P axis and the fault normal is $\gamma = 45° + \alpha/2$. The same applies to the angles between the P and T axes and the slip vector. Therefore, whenever we calculate the fault normal and the slip vector from the orientations of the P and T axes and the source is tensile, we have to take into account inclination α to obtain correct orientations of the fault and the slip.

3. Numerical Modeling

In this section the formulas for the parameters of tensile earthquakes derived in section 2 are applied on synthetically generated data sets of seismic moment tensors. Artificial noise of different levels is superimposed on the moment tensors in order to simulate the properties of the real data. From statistical properties of the retrieved parameters, procedures for discriminating between shear and tensile

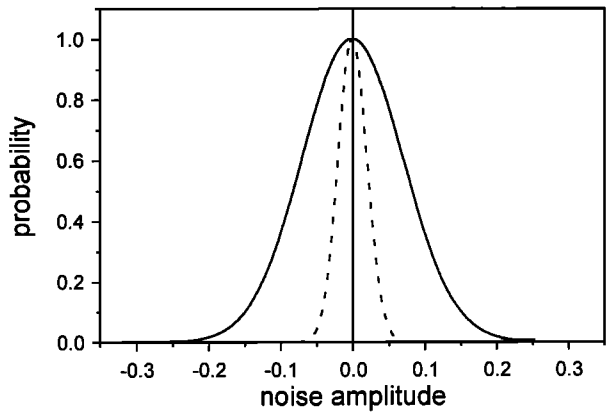

Figure 6. A statistical distribution of noises I (dashed line) and II (solid line).

sources are established. Subsequently, optimum and most accurate procedures for estimating the source parameters of tensile sources are proposed.

3.1. Statistical Properties of the κ Parameter

In order to study the statistical properties of the κ parameter, two data sets each consisting of 1000 events were generated. Such extensive data sets are necessary to draw statistically relevant conclusions. The first data set consists of shear events ($\alpha = 0°$), and the second data set consists of tensile events with a uniform distribution of inclination α in the interval $\alpha \in \langle 5°, 20° \rangle$ and with $\kappa = 0.5$. The moment tensors of both the data sets were superimposed by Gaussian noise of two different levels (noises I and II) defined by the values of parameter σ, 0.02 and 0.07, respectively. The distribution curves of the noise are shown in Figure 6. Noise I can be considered as a rather weak noise, present in well-retrieved moment tensors. Noise II is higher, representing the noise in moment tensors whose retrieval is rather poor. Hence a total of four data sets are processed: two data sets with shear events (with a low and high level of noise) and two data sets of tensile events (also with a low and high level of noise). Subsequently, the moment tensors in the studied data are decomposed into the ISO, CLVD, and DC components and inverted for parameter κ. For the shear events the ISO and CLVD components are fully produced by the noise in the data, and for tensile events the percentages of the ISO, CLVD, and DC are a combination of the noise and tensile mechanisms.

Figure 7 displays the statistical properties of the κ parameter for all data sets under study. It shows that even a small contamination of the moment tensors for shear events results in a quite random behavior of the κ parameter. The random distribution of the κ parameter is independent of the level of the noise. The maximum of the distribution function is at value $\kappa = -2/3$, which is the lowest limit for physically acceptable values of κ. The distribution function is symmetric, implying that the value of κ is unphysical for almost half of the events. This is a strong indication that equation (1) used in the inversion is not appropriate for these data and that the events are in fact noisy shear events. On the contrary, the behavior of the κ parameter for tensile events is quite different. No event displays values $\kappa < -2/3$ for noise I. For noise II an overwhelming majority of events also displays physically acceptable values of κ.

3.2. Consistency Parameter c

A quantitative criterion for discriminating noisy moment tensors of shear and tensile sources can be established by introducing consistency parameter c:

$$c = \frac{N_1}{N_2}, \tag{16}$$

where N_1 is the number of events with $\kappa < -2/3$ (unphysical values, inconsistent with the stability conditions) and N_2 is the number of events with $\kappa \geq -2/3$ (physical values, consistent with the stability conditions). Obviously, the sum of N_1 and N_2 yields the total number N of events in the studied data set. The value of the c parameter can indicate whether the events are shear or tensile. If c is close to or higher than unity, the data consist of shear events. If c is low or equal to zero, then the data consist rather of tensile events. Obviously, for more extensive data sets this indication is more relevant.

In order to study the behavior of the c parameter in detail, the following numerical modeling is performed. Twenty-five data sets are generated each containing moment tensors for 5000 events. The events of each data set display the same value of inclination α. Hence all data sets cover the values of α from 0° to 12° in steps of 0.5°. The value of the κ parameter is 0.5. Similar to the previous numerical experiment, all moment tensors are superposed by noise of two levels (noises I and II, see Figure 6).

Figure 8 shows the c parameter as a function of inclination α. Figure 8 indicates that for shear events the c parameter is approximately unity for both levels of noise. However, when α increases, the c parameter drops very rapidly to zero. For example, for tensile events with $\alpha = 3°$, $c = 0.02$ if the noise is low, and $c = 0.4$ if the noise is high. For high noisy moment tensors of events with $\alpha = 7°$ the c parameter is <0.1.

3.3. Estimation of the Optimum Value of the κ Parameter for Tensile Events

Once it has been proved that the data set consists of tensile events, the optimum value of the κ parameter can be estimated. We can proceed in the three following ways. First, the κ parameter is calculated using (12) and then the standard formula for averaging is applied. Second, instead of the average of κ, the median of κ can be calculated. Third, we can apply (14) in the following way:

$$\kappa = \frac{4}{3}\left(\frac{\sum_{i=1}^{N} \left| c^{\mathrm{ISO}} \right|}{\sum_{i=1}^{N} \left| c^{\mathrm{CLVD}} \right|} - \frac{1}{2} \right), \tag{17}$$

where N is the total number of events in the data set. The sum of absolute values of the ISO and CLVD percentages in (17) is used to prevent instabilities of this formula for data sets containing tensile events with both the positive and negative values of inclination α.

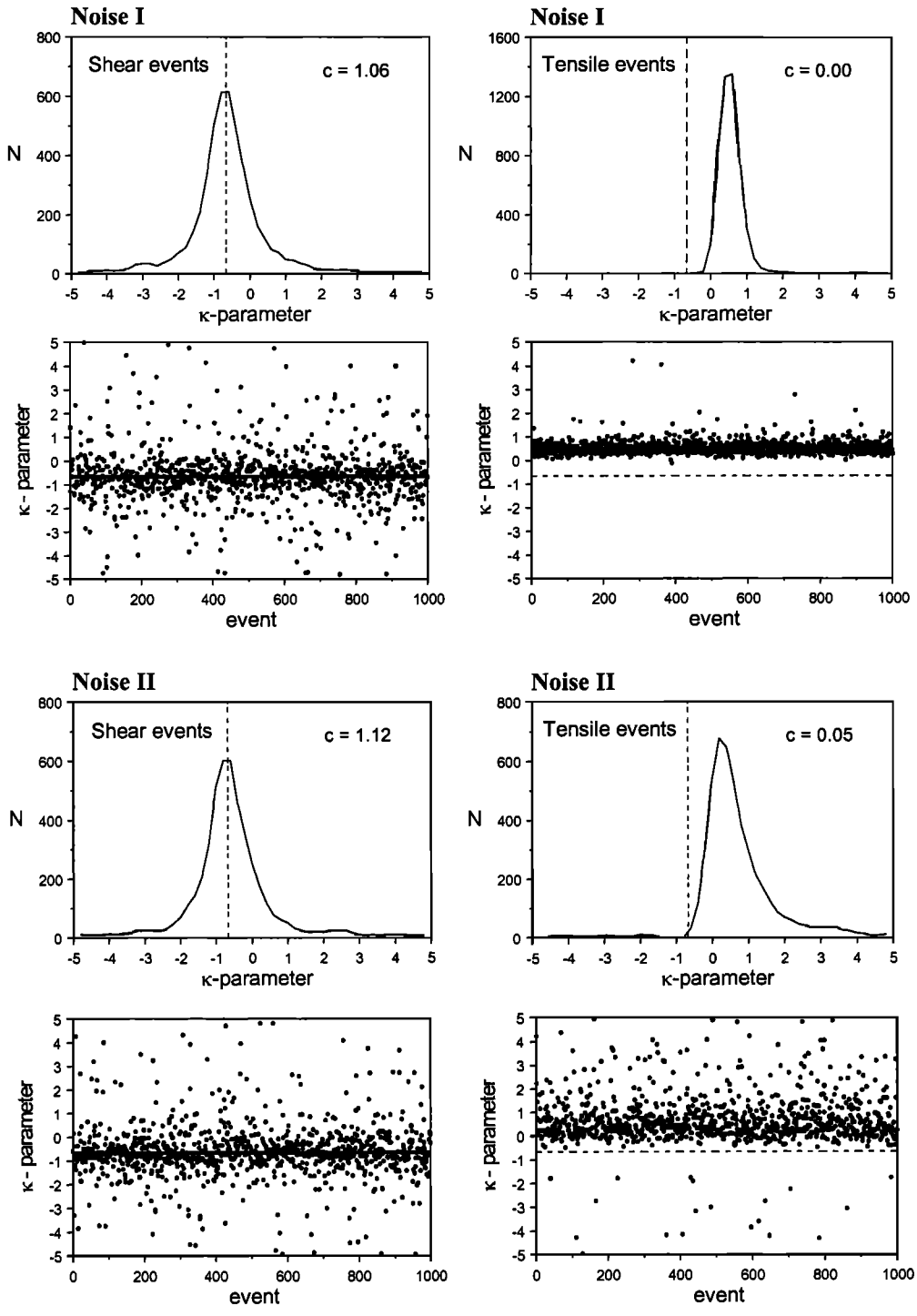

Figure 7. Statistical properties of the κ parameter for the data sets with (left) shear and (right) tensile events. Top four plots show the results for low noisy data, and bottom four plots show the results for high noisy data. The dashed line marks the lowest physically acceptable value of the κ parameter. Quantity c denotes the consistency parameter defined by (16), and N is the number of events.

Figure 9 shows results for all three mentioned approaches tested on the same synthetic data as in the study of the behavior of the c parameter (see Figure 8). The most reliable value of the κ parameter is produced by (17). Equation (17) yields the value of κ with accuracy better than 7% for low noisy events with $\alpha \geq 2°$. The same accuracy is attained for high noisy events with $\alpha \geq 7°$. In both cases, consistency parameter c is ~ 0.1. The median of κ is remarkably less accurate than value produced by (17). However, the worst results are observed for simple averaging of κ. For high noisy data this approach failed completely because it produced the majority of values of κ off the scale in Figure 9.

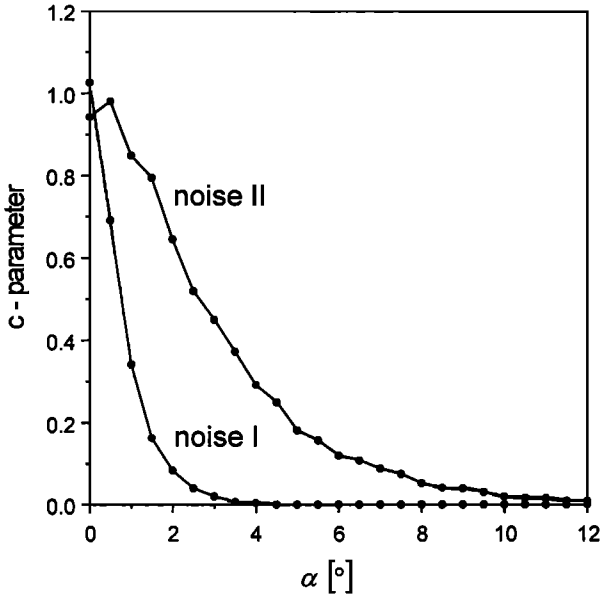

Figure 8. Consistency parameter c as a function of inclination α.

3.4. Resolution of Inclination α

The reliability in retrieving the inclination α is crucial in describing tensile sources. Therefore the accuracy of (13) and (15c) is investigated in this section. The results of (15a) and (15b) are very similar to the results of (15c); hence they are not shown here. To test the accuracy of (13) and (15c) the data sets for tensile events from section 3.1 are used. The data sets contain a broad spectrum of events with inclinations α from 5° to 20°. To calculate α from (15c) the value of κ obtained from (17) was adopted: $\kappa = 0.502$ for low noisy events and $\kappa = 0.524$ for high noisy events (the true value of κ is 0.5).

Table 1. Standard Deviations of the Errors in Inclination α

Method[a]	Low Noisy Data	High Noisy Data
1	±1.27°	±5.05°
2	±1.91°	±6.57°

[a] Method 1 is inclination α calculated by (15c), and method 2 is inclination α calculated by (13).

Table 1 shows standard deviations of the errors in inclination α retrieved by (13) and (15c) for low and high noisy data. Table 1 indicates that (15c) yields a remarkably better resolution of inclination α for both data sets. The application of (15c) yields more accurate and stable results than (13) because (15c) utilizes additional information of the κ parameter. This information is ignored in (13). However, it should be stressed that the higher accuracy achieved by (15c) is due to analyzing homogeneous data sets of events, for which values of the κ parameter are similar for all events. For inhomogeneous data sets the advantage of (15c) will be lost.

3.5. Suppression of Noise in the Data

The numerical tests revealed that a high level of noise significantly deteriorates the resolution of inclination α. Hence a low level of noise in moment tensors is essential for reliable retrieving of α. Therefore a natural intention is to suppress the noise in the data to improve the resolution of the results. For example, the quality of data can be improved by removing extremely noisy values, which are evidently biased from the whole family of the other values. A similar approach can be also applied in retrieving inclination α. In this case, the κ parameter can play the role of a sensitive indicator of noisy data. If we remove events with exceptionally biased values of κ from the data, we can expect the results to be more consistent and accurate. To verify this, the data sets used to calculate inclination α in Figure 7 were modified by selecting only events, which yielded the most reliable values

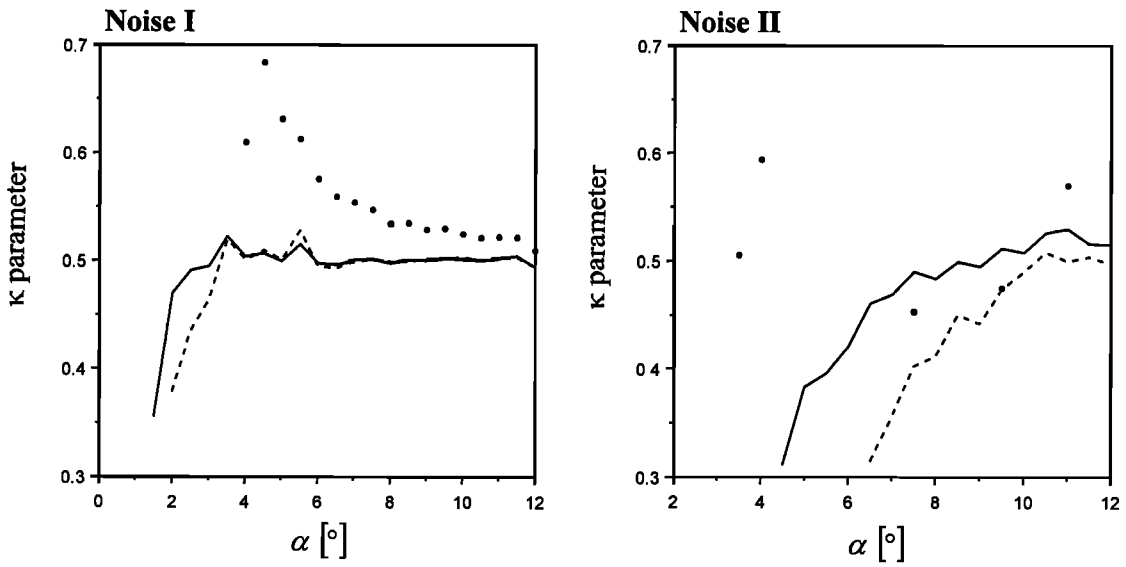

Figure 9. The retrieved optimum value of the κ parameter as a function of inclination α for (left) low noisy and (right) high noisy data. The κ parameter is calculated by standard averaging (dots), by medians (dashed line), and using (17) (solid line). The missing dots for some values of inclination α indicate that these values of κ were off the scale. The true value of κ is 0.5.

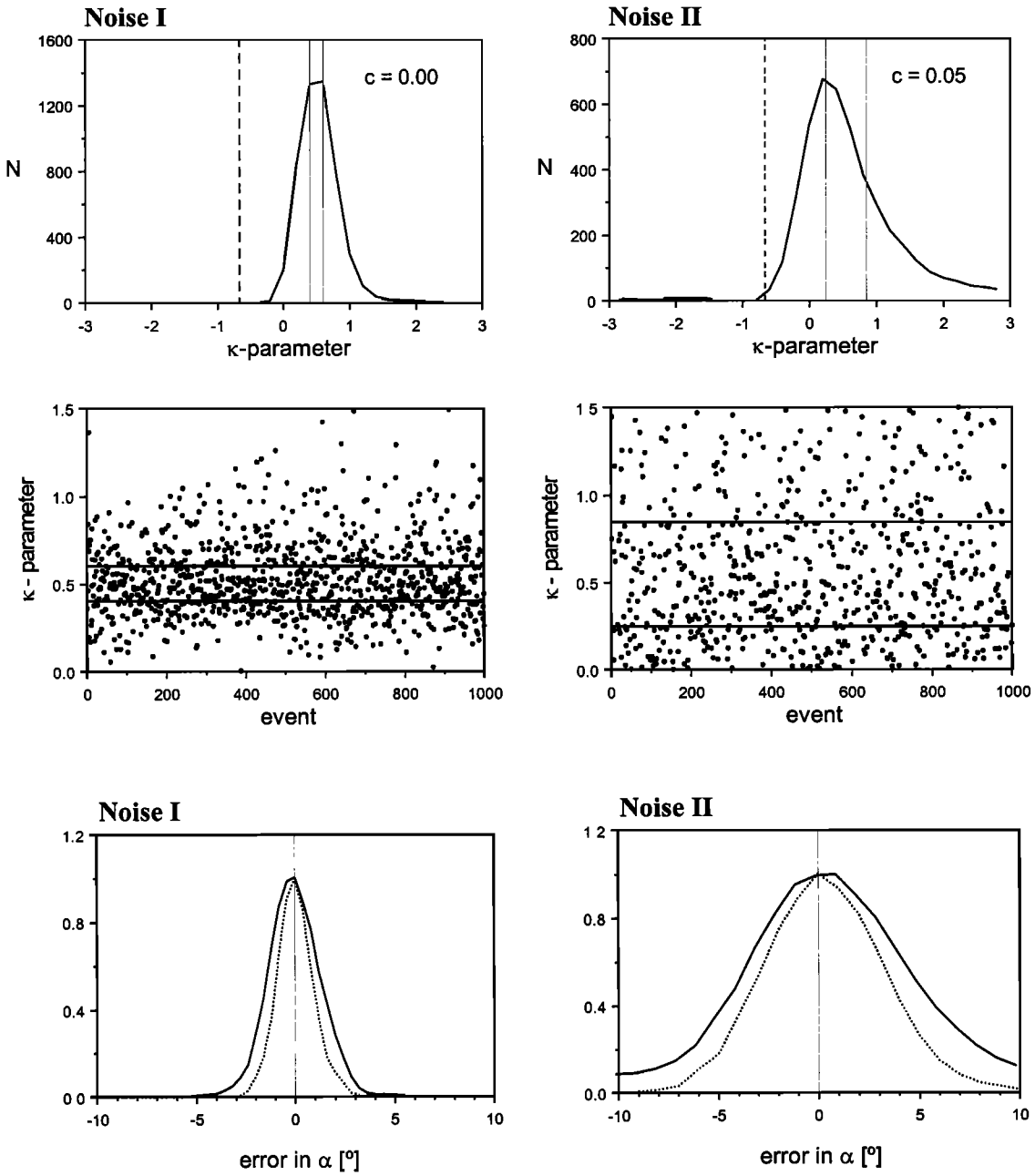

Figure 10. Suppression of noise in the (left) low noisy and (right) high noisy data. Top and middle plots show the statistical distribution of κ for the original data together with the intervals of selected values of κ and bottom plots show a comparison of the errors in inclination α for the original (solid line) and selected (dotted line) data. The dashed line marks the lowest physically acceptable value of κ. The distribution of errors in α is normalized to unity. The distribution functions were smoothed by moving averages.

of κ. The limits for κ were fixed as $0.4 < \kappa < 0.6$ for low noisy data and $0.2 < \kappa < 0.8$ for high noisy data (see Figure 10, top and middle). Of the total number of 1000 events, 388 and 357 events met these criteria. Then the calculation of α was repeated for the reduced data sets. The results of this test are shown in Figure 10 (bottom). Figure 10 confirms that the resolution of α improved for selected data. The standard deviations of errors in α decreased from values 1.27° and 5.05° to values 0.87° and 2.63° for low and high noisy data, respectively. This is a remarkably higher accuracy as compared to the results obtained from the original data.

4. Application to the January 1997 Earthquake Swarm in West Bohemia, Czech Republic

West Bohemia is a seismically active area characterized by the repeated occurrence of earthquake swarms. The seismic activity in the area is probably related to young Quaternary volcanism and deep tectonic processes connected with intrusions of mantle fluids and gases [*Weinlich et al.*, 1998]. One of the strongest recent earthquake swarms occurred in December 1985 and January 1986 [*Vavryčuk*, 1993] and involved more than 7000 microearthquakes, the largest event

being of magnitude 4.6. The January 1997 swarm was considerably weaker. It took place in the epicentral area of Nový Kostel (see Figure 11), which has been the most active area in the region in the past two decades. The swarm lasted for 20 days and consisted of ~ 1800 microearthquakes, the strongest of which was of magnitude 3.0. The hypocentres clustered in a very small volume of < 1 km^3 [*Fischer and Horálek*, 2000] at depths around 9 km. The microearthquakes were recorded by nine local three-component digital broadband (0.5–60 Hz) seismic stations. The sampling rate was 250 Hz, and the dynamic range was 96 dB or more (for details, see *Špičák et al.* [1999] and *Horálek et al.* [2000a]).

4.1. Earthquake Foci and Mechanisms

Horálek et al. [2000b] visually inspected the majority of the recorded events and classified them into several types according to their waveforms. The earthquakes of the two most frequent types were denoted as A and B events. *Fischer and Horálek* [2000] located them using the master event procedure and calculated the orientations of possible fault planes from the alignment of the hypocenters. They suggested that the A and B events were associated with different fault planes (see Figure 12). This finding has been confirmed by comparing the alignment of epicenters in Figure 12 with the preferred nodal plane of the fault plane solutions of the A and B events (see Figure 14 in section 4.2).

Horálek et al. [2000b] selected 70 events of high-quality recordings at six to nine seismic stations and with a signal-to-noise ratio higher than 10. They measured three components of the P and S wave amplitudes of ground displacement seismograms and inverted them for the moment tensors. The Green functions used in the inversion were calculated by the ANRAY program package [*Gajewski and Pšenčík*, 1990] for a one-dimensional (1-D) inhomogeneous isotropic medium with a variable gradient of the P and S wave velocities. Since *Horálek et al.* [2000b] applied the full moment tensor inversion [*Šílený and Pšenčík*, 1995; *Šílený*, 1997, 1998], they provide, besides standard double-couple solutions, also the size of the DC versus non-DC components in the earthquake mechanisms. They found that the A and B events differ also in their focal mechanisms. The A events are oblique normal, and the B events are oblique reverse. The A events are defined by strikes (290°, 315°), dips (40°, 60°), and rakes (-155°, -175°), and the B events have strikes (20°, 60°), dips (55°, 90°), and rakes (35°, 50°). The A and B events display a different percentage of the DC and non-DC components in their mechanisms. The A events display high DC components (from 80% to 100%). The B events display systematically high non-DC components (from 20% to 60%). The non-DC components contain both the ISO and CLVD parts.

The crucial point is to resolve the origin of the non-DC components observed in the B events: whether they are real,

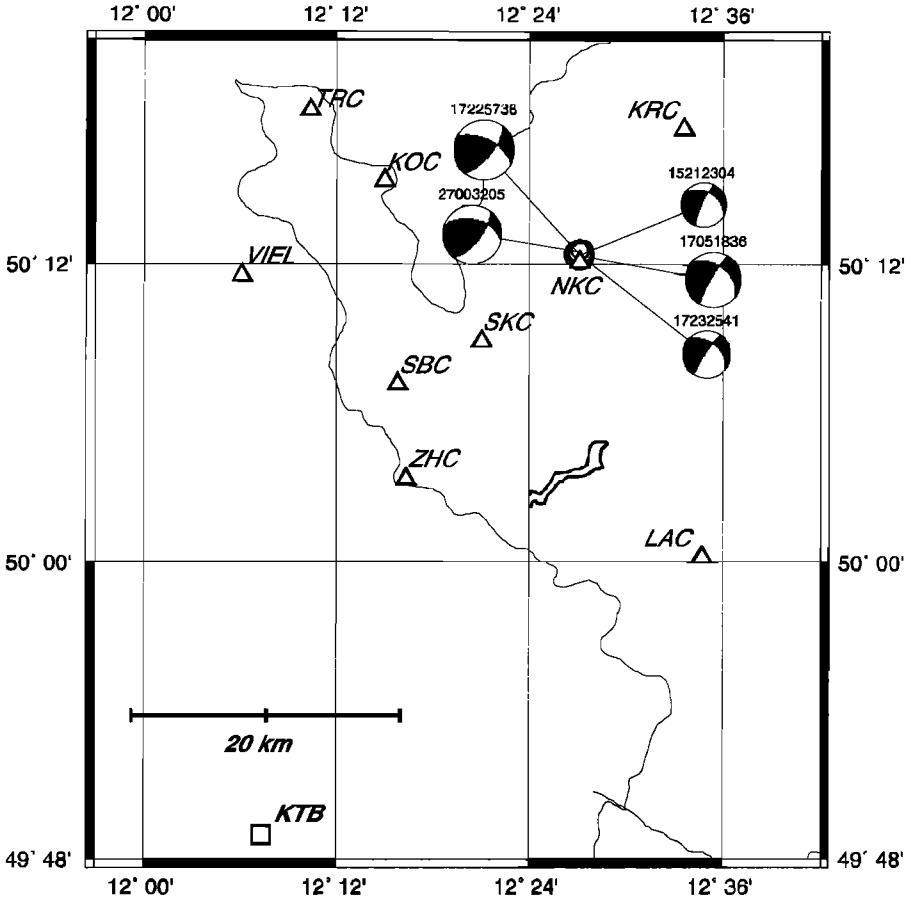

Figure 11. Map of the West Bohemia earthquake swarm region [after *Dahm et al.*, 2000]. The seismic area Nový Kostel (NKC) is marked by the circle. Triangles denote positions of the local seismic stations. The double-couple mechanisms of five stronger events are plotted. The border between the Czech Republic and Germany is shown; KTB gives the location of the deep borehole in Germany.

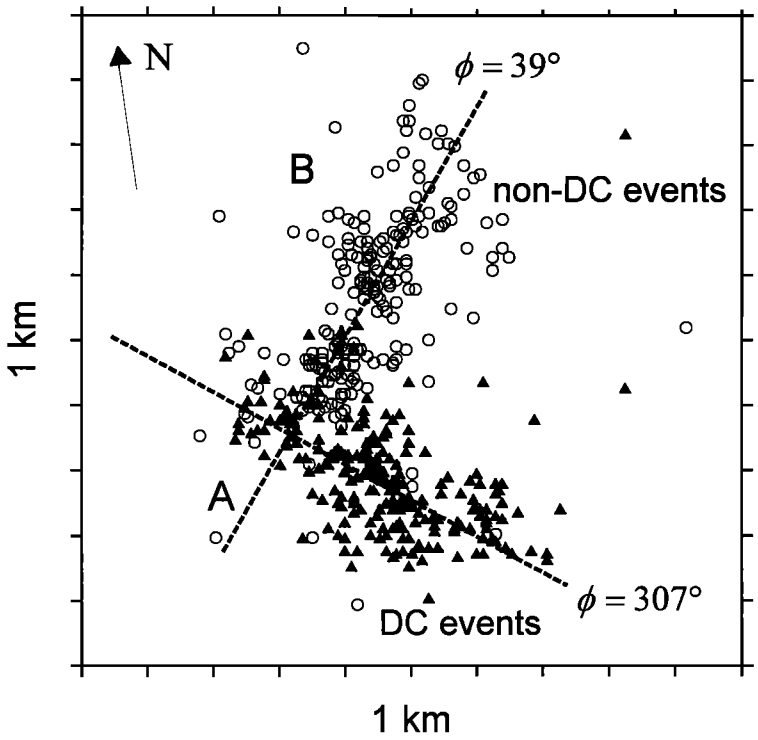

Figure 12. Locations of the A and B events of the January 1997 earthquake swarm. The arrow indicates north. The dashed lines delineate the fault plane orientations estimated by visual interpolation of foci clusters, and ϕ denotes the strike of the fault planes. The triangles and circles denote the A and B events, respectively.

reflecting a specific source process or just errors of the inversion. *Dahm et al.* [2000] explored the accuracy of the mechanisms of the events by a comparison of absolute and relative moment tensor solutions. They also estimated errors in the absolute moment tensors due to inexact selection of amplitudes and inexact modeling of the medium by considering uncertainty in the Q factor. They concluded that the non-DC components in the mechanisms could not be just an artefact of inaccurate moment tensor inversion but that a significant part of these components reflected the actual properties of the source process. Constructing confidence regions of the absolute moment tensors for selected events, they showed that the high DC components in the A events and high non-DC components in the B events were significant at confidence level of 99%.

4.2. Selection of Reliable Data

I used the moment tensors of 20 type A events and 25 type B events calculated by *Dahm et al.* [2000] and *Horálek et al.* [2000b]. Although the moment tensors were carefully determined, they are not free of errors. Numerical modeling has shown that the inversion for tensile parameters is very sensitive to errors in the data. I therefore attempted to suppress the errors in the data set by selecting only the most reliable moment tensors. In order to estimate the quality of the data the results of the two different moment tensor inversions were compared: The inversion performed from both P and S amplitudes [*Dahm et al.*, 2000] and the inversion performed from P amplitudes only. Specifically, orientations of the nodal planes of the double-couple parts for both the inversion methods were compared. The comparison is shown in Figure 13. Figure 13 implies that the mechanisms are very similar for the majority of events: The average deviation of the fault orientation is 10.7°, and the average deviation in the slip direction is 12.5°. This indicates that the results of the inversions are very stable and plausible for most of the events. However, several events display the mechanisms of the two inversions significantly different. This is an indication that these mechanisms are problematic. We can expect that also their ISO, CLVD, and DC components will be problematic because these values are even more sensitive to errors in the moment tensors than the orientation of the double-couple solution [*Šílený and Vavryčuk*, 2000]. In order to separate these anomalous events only the events yielding the sum of the deviations between the fault and slip orientations $<25°$ were retained. This condition was satisfied by 14 type A events and 22 type B events; hence 9 events were discarded (see Figure 13, bottom).

Table 2 gives the list of events selected under the above mentioned criteria. Figure 14 shows the fault plane solutions and Figure 15 shows the histograms of the ISO, CLVD, and DC components in the moment tensors of the events. Figure 15 illustrates the essential differences between the properties of the A and B events reported by *Dahm et al.* [2000] and *Horálek et al.* [2000b]. High DC components are observed for the A events, but strikingly low DC are observed together with high CLVD and ISO components for the B events. This also supports the idea that the A and B events are associated with different fault systems.

4.3. Inversion for the κ Parameter and Inclination α

According to sections 2.4, 3.2. and 3.3. we can calculate consistency parameter c for the 36 selected events and invert

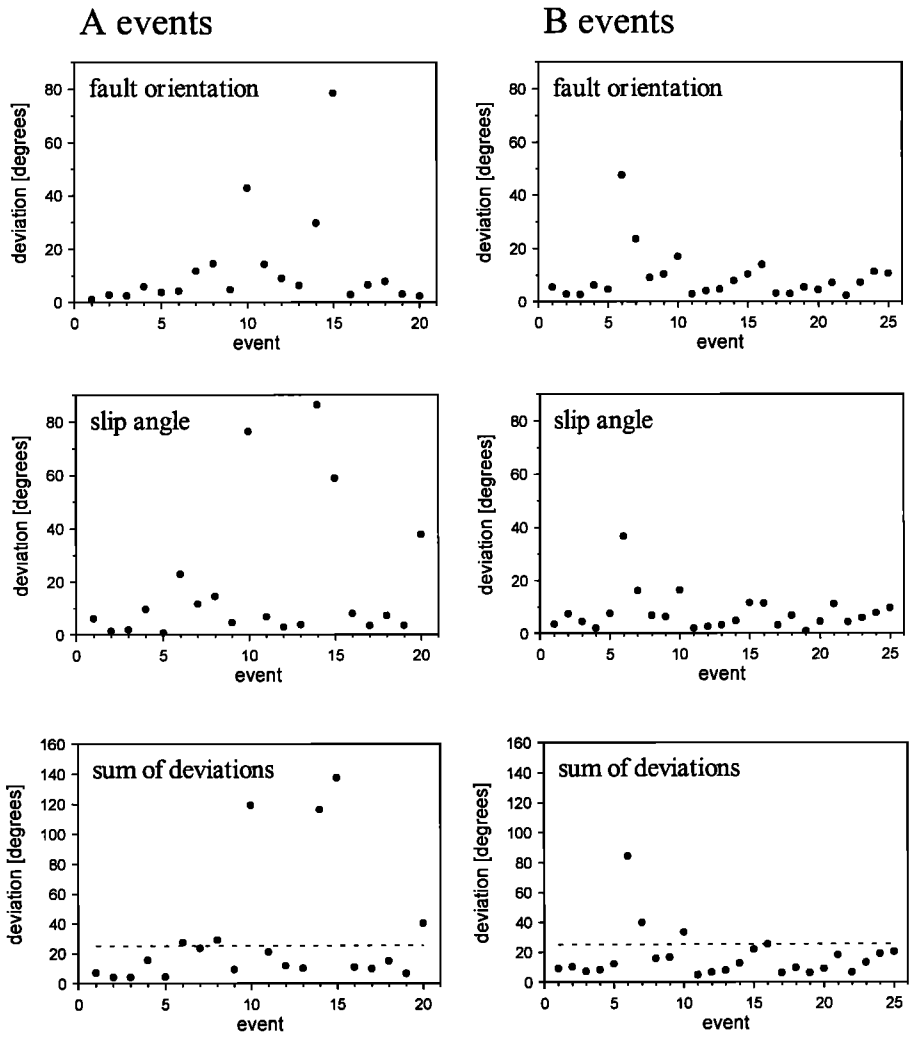

Figure 13. A comparison of focal mechanisms calculated by inverting *P* and *S* amplitudes and by inverting *P* amplitudes only. (top) Differences are shown in the fault orientations, (middle) differences are shown in the slip directions, and (bottom) sum is shown of differences in the fault orientations and slip directions. The dashed line denotes the threshold separating the reliable and unreliable focal mechanisms.

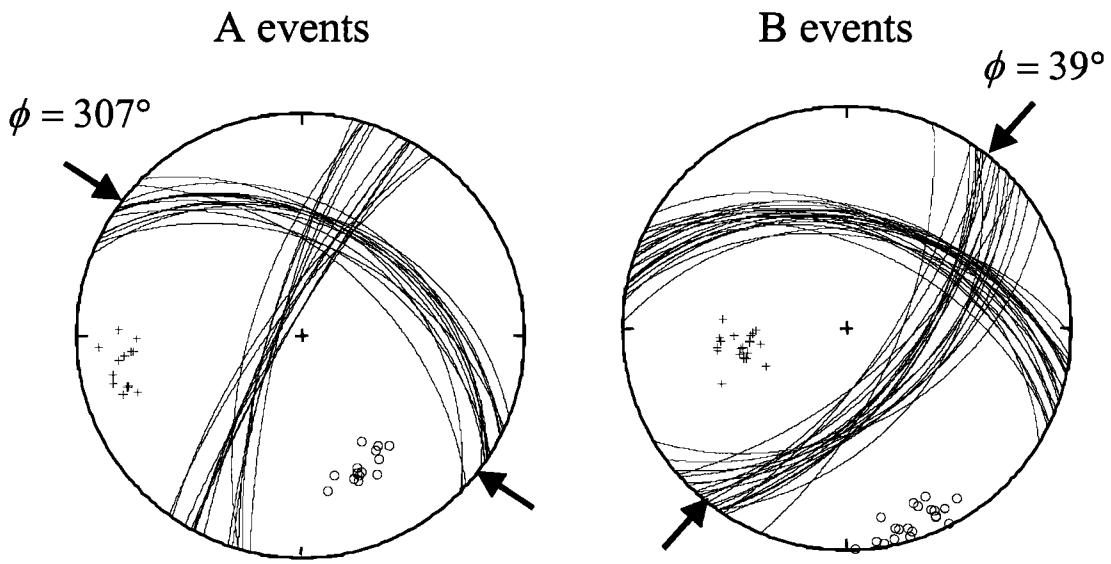

Figure 14. Focal spheres for the selected A and B events with the most reliable mechanisms. The arrows denote the strike of the fault plane measured from the clustering of epicenters (see Figure 12). The circles and pluses denote the *P* and *T* axes, respectively.

Table 2. Earthquakes Used for the Inversion of Parameters of the Tensile Source[a]

No.	Date	Time, UT	Ml	Type	δ, deg	ϕ, deg	λ, deg	ISO, %	DC, %	CLVD, %	κ	α, deg
1	Jan. 15, 1997	0457:13	1.3	A	46	304	-173	5.4	94.3	0.3	25.5	1.6
2	Jan. 15, 1997	0530:28	1.4	A	50	315	-167	-6,3	74.5	-19.1	-0.2	-8.2
3	Jan. 15, 1997	0530:57	1.9	A	43	307	-173	-1.8	86.7	-11.5	-0.5	-4.0
4	Jan. 15, 1997	1219:18	1.9	A	57	302	-169	1,4	98.6	0.0	332.9	0.4
5	Jan. 15, 1997	1810:42	1.5	A	49	305	-170	0.0	96.4	3.6	-0.7	1.0
6	Jan. 15, 1997	2103:53	0.5	A	45	292	-169	0.9	92.0	7.0	-0.5	2.3
7	Jan. 15, 1997	2123:03	1.3	A	47	297	-164	-2.7	94.8	-2.5	0.8	-1.5
8	Jan. 16, 1997	1511:20	2.0	A	61	313	-165	-9.5	71.6	-18.9	0.0	-9.3
9	Jan. 16, 1997	1603:04	0.9	A	49	296	-168	2.3	92.2	5.5	-0.1	2.3
10	Jan. 16, 1997	1612:20	1.1	A	56	295	-170	6.8	81.2	12.0	0.1	5.8
11	Jan. 17, 1997	0518:35	2.0	A	48	304	-174	2.2	95.0	2.8	0.4	1.4
12	Jan. 17, 1997	0753:17	1.1	A	48	304	-155	-4.8	86.3	-8.9	0.1	-4.1
13	Jan. 17, 1997	2147:36	1.4	A	46	297	-164	-3.2	96.5	-0.3	14.7	-1.0
14	Jan. 17, 1997	2325:40	2.3	A	53	305	-170	4.9	92.1	2.9	1.6	2.3
15	Jan. 16, 1997	1650:38	0.7	B	56	50	45	17.8	48.8	33.4	0.0	19.4
16	Jan. 17, 1997	0530:58	0.8	B	74	38	45	15.0	61.3	23.7	0.2	13.3
17	Jan. 17, 1997	0722:37	1.2	B	75	34	45	16.1	70.4	13.6	0.9	9.6
18	Jan. 17, 1997	0909:52	0.9	B	54	60	48	19.0	52.0	29.0	0.2	17.8
19	Jan. 17, 1997	2257:38	3.0	B	67	43	39	9.5	75.3	15.1	0.2	7.7
20	Jan. 18, 1997	0056:15	0.9	B	63	35	45	17.9	46.0	36.1	0.0	21.0
21	Jan. 18, 1997	0108:11	1.2	B	57	46	51	17.3	43.9	38.8	-0.1	22.2
22	Jan. 18, 1997	0534:15	2.3	B	65	41	34	3.3	45.8	50.9	-0.6	21.1
23	Jan. 18, 1997	0551:04	1.6	B	65	35	46	15.1	65.3	19.5	0.4	11.6
24	Jan. 18, 1997	0555:32	1.0	B	60	45	49	15.4	51.8	32.9	0.0	17.9
25	Jan. 18, 1997	0628:08	1.2	B	61	48	50	15.8	52.9	31.3	0.0	17.3
26	Jan. 18, 1997	0958:08	1.9	B	70	40	49	13.0	65.0	22.0	0.1	11.7
27	Jan. 18, 1997	1000:11	0.7	B	66	37	48	17.0	55.0	27.9	0.1	16.2
28	Jan. 18, 1997	1921:01	0.7	B	63	35	46	17.8	49.5	32.7	0.1	19.0
29	Jan. 19, 1997	0525:12	1.0	B	72	49	45	19.2	62.0	18.8	0.7	13.0
30	Jan. 19, 1997	1457:14	0.8	B	54	35	48	19.7	41.1	39.1	0.0	23.9
31	Jan. 26, 1997	1231:27	1.1	B	57	54	48	15.0	79.9	5.1	3.3	6.1
32	Jan. 26, 1997	1445:58	1.6	B	70	33	42	12.2	72.7	15.1	0.4	8.7
33	Jan. 26, 1997	1454:37	0.9	B	58	43	44	18.7	44.6	36.7	0.0	21.8
34	Jan. 27, 1997	0032:04	2.0	B	65	37	49	14.0	62.8	23.2	0.1	12.7
35	Jan. 27, 1997	0059:53	0.9	B	71	23	37	13.8	68.8	17.4	0.4	10.2
36	Jan. 27, 1997	1325:14	0.8	B	64	33	47	15.8	62.3	21.8	0.3	12.9
Average values for the A events					50	303	-168	-0.3	89.4	-1.9	26.7	-0.8
Average values for the B events					64	41	46	15.4	58.0	26.6	0.3	15.2

[a] Angles δ, ϕ, and λ mean dip, strike and rake of the fault plane solution.

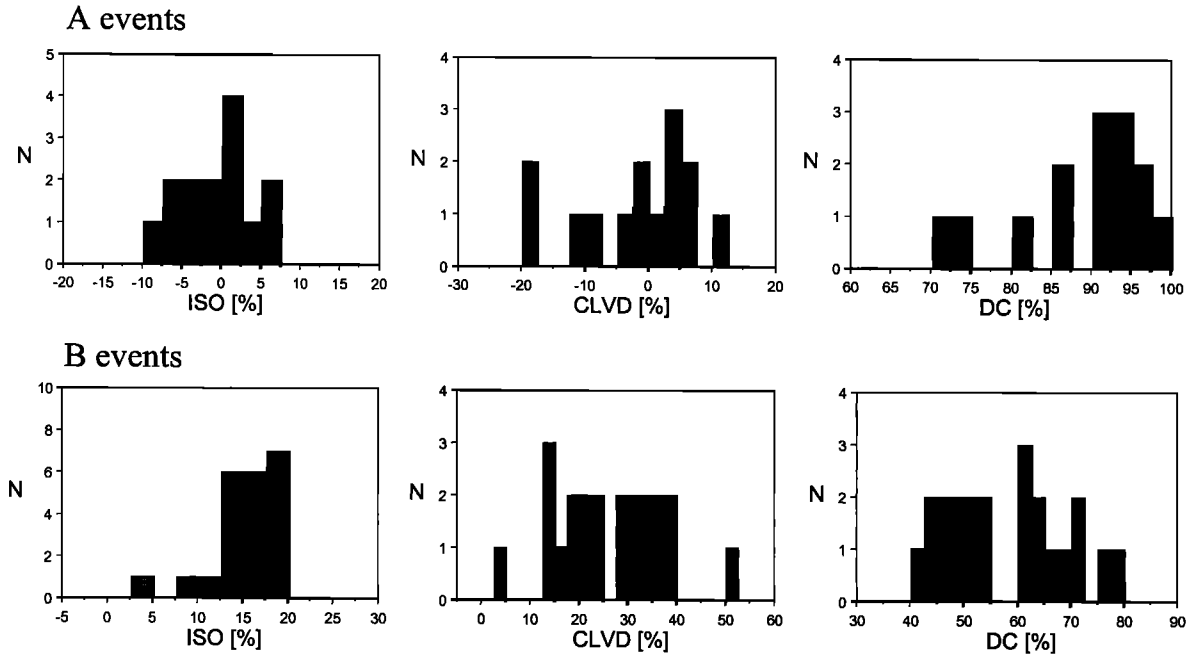

Figure 15. Histograms of the percentages of the ISO, CLVD, and DC components calculated by the decomposition of the moment tensors for selected events.

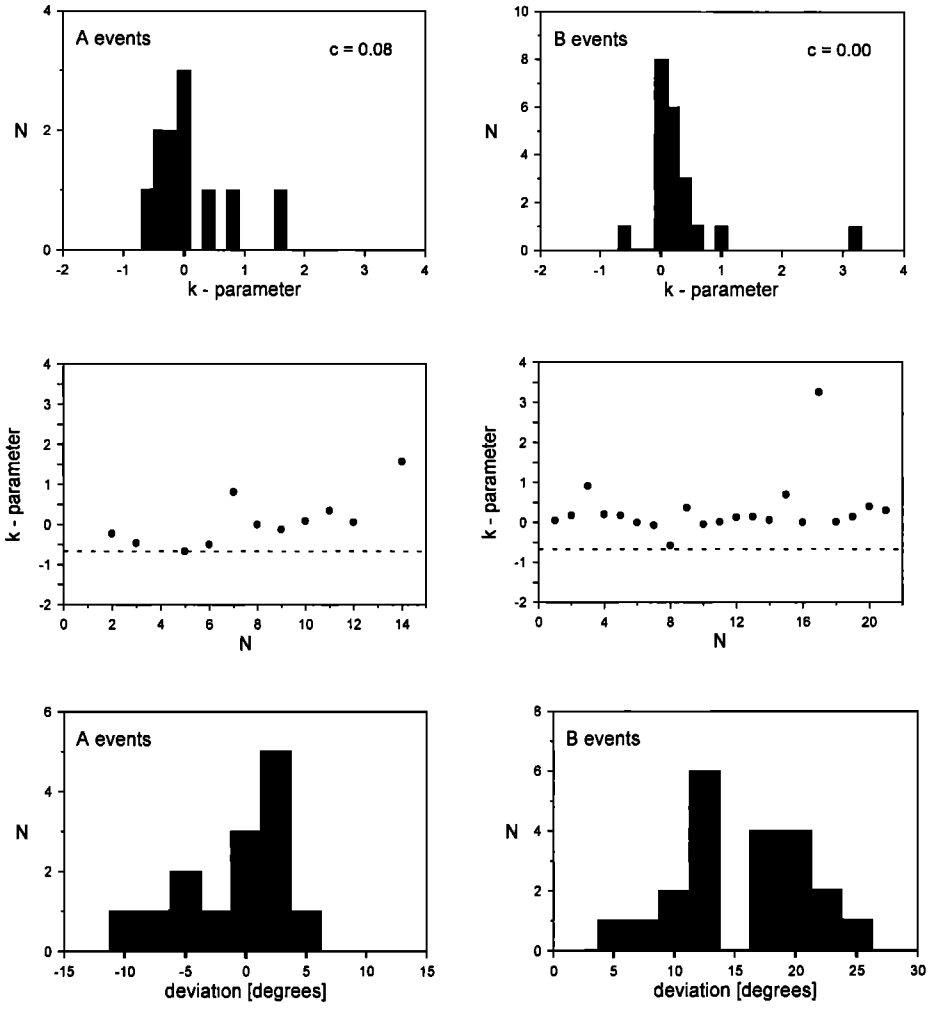

Figure 16. The κ parameter and inclination α for the A and B events. Quantity c is the consistency parameter calculated by (16).

the moment tensors to obtain the κ parameter and inclination α. Unfortunately, the number of events is rather low; hence we cannot expect to achieve very accurate statistical results. The results of the inversion are shown in Figure 16. Except for one A event, all events have physically acceptable values of the κ parameter. However, the values of κ for the A events display higher scatter than for the B events (see Table 2). The optimum value of κ calculated using (17) is 0.06 for the A events and 0.11 for the B events. The median of κ yields a value of 0.10 for both types of events. For the simple averages of κ, see Table 2. The low values of the consistency parameter c together with acceptable optimum values of the κ parameter are strong indications that the data analyzed indeed represent events with well-retrieved moment tensors and that the source model described by (1) is appropriate for the majority of these events. The histogram of values of inclination α shows that the A events are characterized by small α, thus being close to shear faulting. This explains the high scatter of the κ parameter for the A events because the retrieval of the κ parameter is more difficult for nearly shear sources than for tensile sources (see Figure 7). It follows from Figure 16 that some of the A events display small tensile ($0° < \alpha < 5°$) or compressive ($-10° < \alpha < 0°$) components. On the other hand, all B events are tensile, and the majority of them display inclination α in the interval $10° < \alpha < 20°$. The accuracy of α can be estimated from a comparison of statistical distributions of the κ parameter for the real data (see Figure 16, top) and the synthetic data (see Figure 7). This comparison indicates that the errors in the moment tensors for the A and B events are higher than those for the synthetic tensile events with noise I but less than for the events with noise II. Therefore the deviation σ of inclination α is likely to be less than 4° ($\sigma = 1.27°$ and 5.05° for noises I and II, respectively). Hence the non-DC components of the B events cannot be a product of errors in the moment tensors due to an inaccurate inversion, but they arise from the tensile nature of faulting.

4.4. Physical Explanation of Tensile Earthquakes

In order to understand the differences in faulting of the A and B events and, in particular, causes of tensile faulting for the B events, we have to know the stress in the focal region and to analyze the forces acting on the fault. The stress is calculated from the focal mechanisms of earthquakes under study (see Table 2) by applying the inversion method of *Gephart and Forsyth* [1984] (see also *Michael* [1987], *Gephart* [1990], and *Lund and Slunga* [1999]). This method

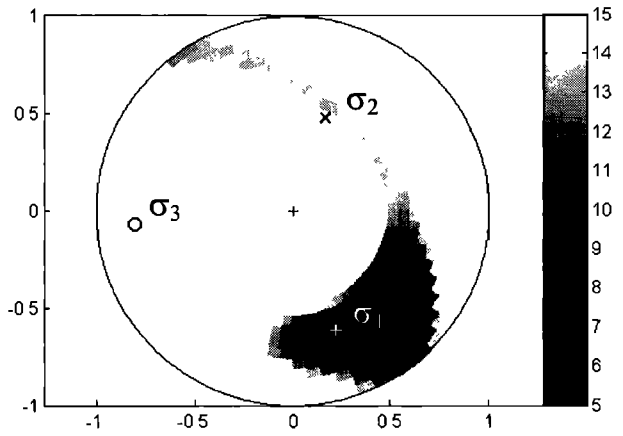

Figure 17. Inversion for the stress tensor. The misfit function for the σ_1 direction (average of deviations between the projection of the slip and shear traction on the fault measured in degrees) is displayed for the whole lower hemisphere. Equal-area projection is used.

assumes (1) that the stress is uniform in the region under study, (2) that the earthquakes occur on pre-existing faults, and (3) that the slip vector projected into the fault points in the direction of the resolved shear traction on the fault. The stress tensor is searched to minimize the sum of deviations between the shear traction directions and observed projections of the slips at the faults. The misfit function is minimized by using the robust grid search inversion scheme. We can recover three angles defining the directions of the three principal stress axes and parameter $R=(\sigma_1-\sigma_2)/(\sigma_1-\sigma_3)$, which bounds the size of the maximum, intermediate, and minimum compressive principal stresses σ_1, σ_2, and σ_3. This method is unable to recover the magnitudes of the principal stresses and the isotropic part of the stress tensor $\sigma^{ISO}=\sigma_1+\sigma_2+\sigma_3$. The inversion for the optimum stress tensor was performed by using a 5° grid in searching through the principal stress directions and a 0.05 increment in searching for σ_2. Figure 17 shows the results of this inversion. The optimum stress tensor is defined by the stress directions (plunge/azimuth): $\sigma_1=35°/160°$, $\sigma_2=48°/19°$, $\sigma_3=20°/265°$, and $R=0.76$. The plunge is measured from the horizontal plane, and the azimuth is measured clockwise from north. The average deviation angle is 5.1°. It is worth noting that the azimuth of the resolved maximum compressive stress coincides well with the mean orientation of the stress in western Europe [*Müller et al.*, 1992]: N144°E±26°, but the resolved stress significantly deviates from the horizontal direction.

Using the stress determined and focal mechanisms from Table 2, we can analyze the forces on the faults for the A and B events by constructing Mohr's circle diagram (see Figure 18). Figure 18 shows the relationship between the shear and normal tractions along the fault under a specified stress [see *Mavko et al.*, 1998]. It follows from Figure 18 that the A and B earthquakes are generated under different stress conditions along the fault. Normal traction is compressive for most of the A events, and shear traction is very close to its maximum value available in the stress field. This explains the predominance of the DC component in the A events and the very low and rather compressive non-DC component. Normal traction is tensile for the B events, and shear traction is considerably lower than for the A events. This is again perfectly consistent with the tensile nature of faulting for the B events. Note that tensile faulting is physically permissible under the condition that high fluid pressure is present at the fault because this pressure can reduce the compressive lithostatic stress at the fault [*Julian et al.*, 1998]. The condition of high fluid pressure is a reasonable assumption satisfied in the area under study [see *Špičák et al.*, 1999]. This is also supported by the fact that the A events that were rather compressive occurred mainly in the beginning of the swarm. Hence they could induce an increase of fluid pressure and prepare conditions for a successive occurrence of the tensile B events. The B events occurred in later phases of the swarm and could cause a partial relaxation of fluid pressure.

5. Summary

The main results of the paper are summarized as follows:

1. The formulas proposed for calculating the percentages of ISO, CLVD, and DC components are suitable for studying tensile sources. These formulas yield the constant ISO/CLVD ratio irrespective of the inclination of the slip vector from the fault.

2. The λ/μ ratio at the fault has been denoted as the κ parameter and distinguished from the λ/μ ratio in the medium evaluated from P and S velocities. The optimum

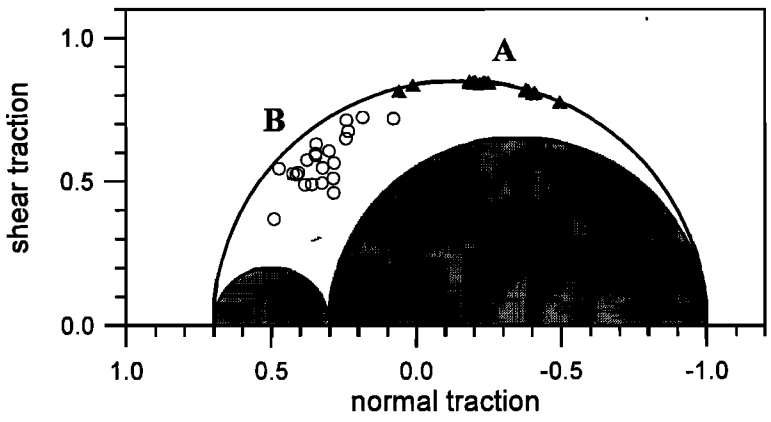

Figure 18. Mohr's circle diagram. The triangles and circles denote the A and B events, respectively. All permissible values of shear and normal tractions must lie inside the large circle but outside of the shaded area.

value of κ can be calculated using the ISO and CLVD percentages for a set of moment tensors. The κ parameter is likely to play an important role in future detailed studies of physical conditions along a fault.

3. The consistency parameter c has been introduced. This parameter is calculated from numbers of physically realistic and unrealistic values of κ, and it serves as a criterion for discriminating the noisy moment tensors of shear earthquakes from those of tensile earthquakes. If c approaches unity, the moment tensors describe noisy DC events and if c is close to zero, the moment tensors describe tensile events.

4. The inclination α of the slip vector from the fault can be calculated from the ISO, CLVD, and DC percentages. The proposed formula for α produces less scattered results as compared with the previously published formulas, provided the analyzed data sets consist of earthquakes with similar values of κ.

5. The κ parameter is very sensitive to noise in moment tensors. This can be utilized for suppressing errors in the studied data set and for enhancing the accuracy of the retrieved inclination of the slip vector from the fault.

6. The standard procedures for calculating the fault orientation and slip direction are valid for shear sources, but they yield biased results for tensile sources. Therefore, whenever tensile earthquakes are detected, the fault orientation and the slip direction retrieved must be corrected. This correction is calculated from the orientation of the P and T axes and from inclination α.

7. The DC percentage is very sensitive to inclination α. A reduction of the DC percentage to 50-60% can be successfully explained by tensile faulting with the slip inclination being only of 20°.

8. Some of earthquakes which occurred during the January 1997 earthquake swarm in West Bohemia, Czech Republic, displayed tensile faulting. The optimum value of the κ parameter was close to zero (~0.1). The inclination α of the slip vector from the fault attained values ranging from -10° up to 20° with a standard deviation of 4°. The tensile nature of the earthquakes was caused by tensile normal traction and reduced shear traction along the fault and by presence of high-fluid pressure in the region. The majority of earthquakes with slightly compressive faulting preceded earthquakes with tensile faulting.

Acknowledgments. I thank A. Plešinger and J. Šílený for critically reading the manuscript and for their comments. I thank T. Fischer for providing me with the refined locations of the A and B events shown in Figure 12 and T. Dahm for giving his permission for reproduction of Figure 11. This work was partially performed at CPGG/UFBA, Salvador, Brazil, where the author was a visiting professor. The work was supported by the agencies CNPq and PGS of Brazil, and by the Grant Agency of Academy of Sciences of the Czech Republic, grant A3012904.

References

Aki, K., and P. G. Richards, *Quantitative Seismology: Theory and Methods*, W. H. Freeman, New York, 1980.

Anooshehpoor, A., and J. N. Brune, Frictional heat generation and seismic radiation in a foam rubber model of earthquakes, *Pure Appl. Geophys., 142*, 735-747, 1994.

Backus, G. E., Long-wave anisotropy produced by horizontal layering, *J. Geophys. Res., 66*, 4427-4440, 1962.

Brace, W. F., B. W. Paulding Jr., and C. H. Scholz, Dilatancy in the fracture of crystalline rocks, *J. Geophys Res., 71*, 3939-3953, 1966.

Brune, J. N., S. Brown, and P. A. Johnson, Rupture mechanism and interface separation in foam rubber models of earthquakes: A possible solution to the heat flow paradox and the paradox of large overthrusts, *Tectonophysics, 218*, 59-67, 1993.

Dahm, T., Relative moment tensor inversion based on ray theory: Theory and synthetic tests, *Geophys. J. Int., 124*, 245-257, 1996.

Dahm, T., J. Horálek, and J. Šílený, Comparison of absolute and relative moment tensor solutions for the January 1997 West Bohemia earthquake swarm, *Stud. Geophys. Geod., 44*, 233-250, 2000.

Dufumier, H., and L. Rivera, On the resolution of the isotropic component in moment tensor, *Geophys. J. Int., 131*, 595-606, 1997.

Fischer, T., and J. Horálek, Refined locations of the swarm earthquakes in the Nový Kostel focal zone and spatial distribution of the January 1997 swarm in Western Bohemia, Czech Republic, *Stud. Geophys. Geod., 44*, 210-226, 2000.

Foulger, G. R., Hengill Triple Junction, SW Iceland, 1, Tectonic structure and the spatial and temporal distribution of local earthquakes, *J. Geophys. Res., 93*, 13,493-13,506, 1988a.

Foulger, G. R., Hengill Triple Junction, SW Iceland, 2, Anomalous earthquake focal mechanisms and implications for processes within the geothermal reservoir at accretionary plate boundaries, *J. Geophys. Res., 93*, 13,507-13,523, 1988b.

Frohlich, C., Earthquakes with non-double-couple mechanisms, *Science, 264*, 804-809, 1994.

Gajewski, D., and I. Pšenčík, Vertical seismic profile synthetics by dynamic ray tracing in laterally varying layered anisotropic structures, *J. Geophys. Res., 95*, 11,301-11,315, 1990.

Gephart, J. W., Stress and the direction of the slip on fault planes, *Tectonics, 9*, 845-858, 1990.

Gephart, J. W., and D. W. Forsyth, An improved method for determining the regional stress tensor using earthquake focal mechanism data: Application to the San Fernando earthquake sequence, *J. Geophys. Res., 89*, 9305-9320, 1984.

Horálek, J., T. Fischer, A. Boušková, and P. Jedlička, The Western Bohemia/Vogtland region in the light of the WEBNET network, *Stud. Geophys. Geod., 44*, 107-125, 2000a.

Horálek, J., J. Šílený, T. Fischer, A. Slancová, and A. Boušková, Scenario of the January 1997 West Bohemia earthquake swarm, *Stud. Geophys. Geod., 44*, 491-521, 2000b.

Jost, M. L., and R. B. Hermann, A student's guide to and review of moment tensors, *Seismol. Res. Lett., 60*, 37-57, 1989.

Julian, B. R., A. D. Miller, and G. R. Foulger, Non-double-couple earthquake mechanisms at the Hengill-Grensdalur volcanic complex, southwest Iceland, *Geophys. Res. Lett., 24*, 743-746, 1997.

Julian, B. R., A. D. Miller, and G. R. Foulger, Non-double-couple earthquakes, 1, Theory, *Rev. Geophys., 36*, 525-549, 1998.

Knopoff, L., and M. J. Randall, The compensated linear vector dipole: A possible mechanism for deep earthquakes, *J. Geophys. Res., 75*, 4957-4963, 1970.

Kuge, K., and T. Lay, Data-dependent non-double-couple components of shallow earthquake source mechanisms: Effects of waveform instability, *Geophys. Res. Lett., 21*, 9-12, 1994.

Lund, B., and R. Slunga, Stress tensor inversion using detailed microearthquake information and stability constraints: Application to Ölfus in southwest Iceland, *J. Geophys. Res., 104*, 14,947-14,964, 1999.

Mavko, G., T. Mukerji, and J. Dvorkin, *The Rock Physics Handbook*, Cambridge Univ. Press, New York, 1998.

Michael, A. J., Use of focal mechanisms to determine stress: A control study, *J. Geophys. Res., 92*, 357-368, 1987.

Miller, A. D., G. R. Foulger, and B. R. Julian, Non-double-couple earthquakes, 2, Observations, *Rev. Geophys., 36*, 551-568, 1998.

Müller, B., M. L. Zoback, K. Fuchs, L. Mastin, S. Gregersen, N. Pavoni, O. Stephansson, and C. Ljunggren, Regional patterns of tectonic stress in Europe, *J. Geophys. Res., 97*, 11,783-11,803, 1992.

Ross, A., G. R. Foulger, and B. R. Julian, Non-double-couple earthquake mechanisms at The Geysers geothermal area, California, *Geophys. Res. Lett., 23*, 877-880, 1996.

Scholz, C. H., *The Mechanics of Earthquakes and Faulting*, Cambridge Univ. Press, New York, 1990.

Shimizu, H., S. Ueki, and J. Koyama, A tensile-shear crack model for the mechanism of volcanic earthquakes, *Tectonophysics*, *144*, 287-300, 1987.

Šílený, J., Moment tensor rate functions from waveforms with non-homogeneous variance, *Geophys. J. Int.*, *131*, 767-769, 1997.

Šílený, J., Earthquake source parameters and their confidence regions by a genetic algorithm with "memory", *Geophys. J. Int.*, *134*, 228-242, 1998.

Šílený, J., and I. Pšenčík, Mechanism of local earthquakes in 3-D inhomogeneous media determined by waveform inversion, *Geophys. J. Int.*, *121*, 459-474, 1995.

Šílený, J., and V. Vavryčuk, Approximate retrieval of the point source in anisotropic media: Numerical modelling by indirect parametrization of the source, *Geophys. J. Int.*, *143*, 700-708, 2000.

Sipkin, S. A., Interpretation of non-double-couple earthquake mechanisms derived from moment tensor inversion, *J. Geophys. Res.*, *91*, 531-547, 1986.

Špičák, A., Laboratory investigation into off-fault seismic activity, *Bull. Seism. Soc. Am.*, *78*, 1232-1242, 1988.

Špičák, A., J. Horálek, A. Boušková, Č. Tomek, and J. Vaněk, Magma intrusions and earthquake swarm occurrence in the western part of the Bohemian Massif, *Stud. Geophys. Geod.*, *43*, 87-106, 1999.

Vavryčuk, V., Crustal anisotropy from local observations of shear-wave splitting in West Bohemia, Czech Republic, *Bull. Seism Soc. Am.*, *83*, 1420-1441, 1993.

Walter, W. R., and J. N. Brune, Spectra of seismic radiation from tensile crack, *J. Geophys. Res.*, *98*, 4449-4459, 1993.

Weinlich, F. H., J. Tesař, S. M. Weise, K. Bräuer, and H. Kämpf, Gas flux distribution in mineral springs and tectonic structure in the western Eger Rift, *J. Czech Geol. Soc.*, *43*, 91-110, 1998.

V.Vavryčuk, Geophysical Institute, Bočni II/1401, 141 31 Prague 4, Czech Republic. (vv@ig.cas.cz)

(Received July 6, 2000; revised November 28, 2000; accepted March 20, 2001.)